Kinetic and Chemical Mechanism of α-Isopropylmalate Synthase from *Mycobacterium tuberculosis*†

Luiz Pedro S. de Carvalho and John S. Blanchard*

Department of Biochemistry, Albert Einstein College of Medicine, 1300 Morris Park Avenue, Bronx, New York 10461

Received April 4, 2006; Revised Manuscript Received May 16, 2006

ABSTRACT: *Mycobacterium tuberculosis* α-isopropylmalate synthase (*Mt*IPMS) catalyzes the condensation of acetyl-coenzyme A (AcCoA) with α-ketoisovalerate (α-KIV) and the subsequent hydrolysis of α-isopropylmalyl-CoA to generate the products CoA and α-isopropylmalate (α-IPM). This is the first committed step in L-leucine biosynthesis. We have purified recombinant *Mt*IPMS and characterized it using a combination of steady-state kinetics, isotope effects, isotopic labeling, and ^{1}H-NMR spectroscopy. The α-keto acid specificity of the enzyme is narrow, and the acyl-CoA specificity is absolute for AcCoA. In the absence of α-KIV, *Mt*IPMS does not enolize the α protons of AcCoA but slowly hydrolyzes acyl-CoA analogues. Initial velocity studies, product inhibition, and dead-end inhibition studies indicate that *Mt*IPMS follows a nonrapid equilibrium random bi-bi kinetic mechanism, with a preferred pathway to the ternary complex. *Mt*IPMS requires two catalytic bases for maximal activity (both with pK_a values of ca. 6.7), and we suggest that one catalyzes deprotonation and enolization of AcCoA and the other activates the water molecule involved in the hydrolysis of α-isopropylmalyl-CoA. Primary deuterium and solvent kinetic isotope effects indicate that there is a step after chemistry that is rate-limiting, although, with poor substrates such as pyruvate, hydrolysis becomes partially rate-limiting. Our data is inconsistent with the suggestion that a metal-bound water is involved in hydrolysis. Finally, our results indicate that the hydrolysis of α-isopropylmalyl-CoA is direct, without the formation of a cyclic anhydride intermediate. On the basis of these results, a chemical mechanism for the *Mt*IPMS-catalyzed reaction is proposed.

Mycobacterium tuberculosis, the causative agent of Tuberculosis, is intrinsically resistant to many first-line antibiotics used to treat other common bacterial infections, and resistance to effective drugs is increasing. The characterization of new targets and the development of new drugs are urgently needed. Mycobacteria, like many other bacteria, synthesize the branched-chain amino acids, L-valine and L-leucine, and pantothenic acid from α-ketoisovalerate (α-KIV).[1] Studies using transposon mutagenesis in mycobacteria have demonstrated that the L-leucine biosynthetic pathway is essential for *Mycobacterium bovis* both in vitro and in vivo (*1*−*3*). These results suggest that mycobacteria, engulfed within the macrophage phagolysosome-like compartment, cannot obtain sufficient L-leucine from the surrounding environment. These findings also validate the L-leucine biosynthetic pathway as a target for inhibitor design and drug development to treat Tuberculosis. Despite its importance, the L-leucine biosynthetic pathway is among the least studied of the amino acid biosynthetic pathways.

The L-leucine branch of the branched-chain amino acid pathway (Scheme 1) starts with the acetyl-coenzyme A (AcCoA)-dependent carboxymethylation of α-KIV catalyzed by α-isopropylmalate synthase (IPMS) (EC 2.3.3.13). This enzyme is subject to feedback inhibition by L-leucine in many organisms, and the *M. tuberculosis* α-isopropylmalate synthase (*Mt*IPMS) has recently been shown to exhibit slow-onset, feedback inhibition by L-leucine (*4*). α-Isopropylmalate (α-IPM) is subsequently converted to *β*-isopropylmalate by α-IPM isomerase (EC 4.2.1.33) and then oxidatively decarboxylated to α-ketoisocaproate by *β*-isopropylmalate dehydrogenase (EC 1.1.1.85). α-Ketoisocaproate is converted directly to L-leucine by the action of a branched-chain amino acid transaminase (*5*). All of the genes involved in L-leucine biosynthesis have defined orthologues in the *M. tuberculosis* genome (*6*, *7*).

IPMS catalyzes a Claisen-type condensation between α-KIV and AcCoA. The most well-characterized members of this family are malate synthase (MS), a component of the glyoxylate pathway, citrate synthase (CS), a component of the Krebs cycle, and most recently homocitrate synthase (HCS), a component of the yeast α-aminoadipate pathway (*8*). Despite the similarities in their respective substrates and the chemical reactions catalyzed, MS and CS perform the

† This work was supported by NIH Grant A133696.

* To whom correspondence should be addressed: Department of Biochemistry, Albert Einstein College of Medicine, 1300 Morris Park Avenue, Bronx, NY 10461. Telephone: (718) 430-3096. Fax: (718) 430-8565. E-mail: blanchar@aecom.yu.edu.

[1] Abbreviations: *Mt*IPMS, *M. tuberculosis* α-isopropylmalate synthase; TEA, triethanolamine; HEPES, *N*-[2-hydroxyethyl]piperazine-*N*′-[2-ethanesulfonic acid]; TAPS, *N*-tris[hydroxymethyl]methyl-2-aminopropanesulfonic acid; MES, 2-(*N*-morpholino)ethanesulfonic acid; CHES, 2-(*N*-cyclohexylamino)ethanesulfonic acid; PIPES, piperazine-*N*,*N*′-bis[2-ethanesulfonic acid]; Tris, tris(hydroxymethyl)aminomethane; α-KIV, α-ketoisovalerate; α-KB, α-ketobutyrate; α-KV, α-ketovalerate; PY, pyruvate; α-IPM, α-isopropylmalate; α-HIV, α-hydroxyisovalerate; CoA, coenzyme A; AcCoA, acetyl-coenzyme A; MS, malate synthase; CS, citrate synthase; HCS, homocitrate synthase; DTP, 4,4′-dithiodipyridine; IC_{50}, concentration of the inhibitor necessary to cause 50% loss in activity; NMR, nuclear magnetic resonance; KIE, kinetic isotope effect.

10.1021/bi0606602 CCC: $33.50
Published on Web 06/30/2006

Scheme 1

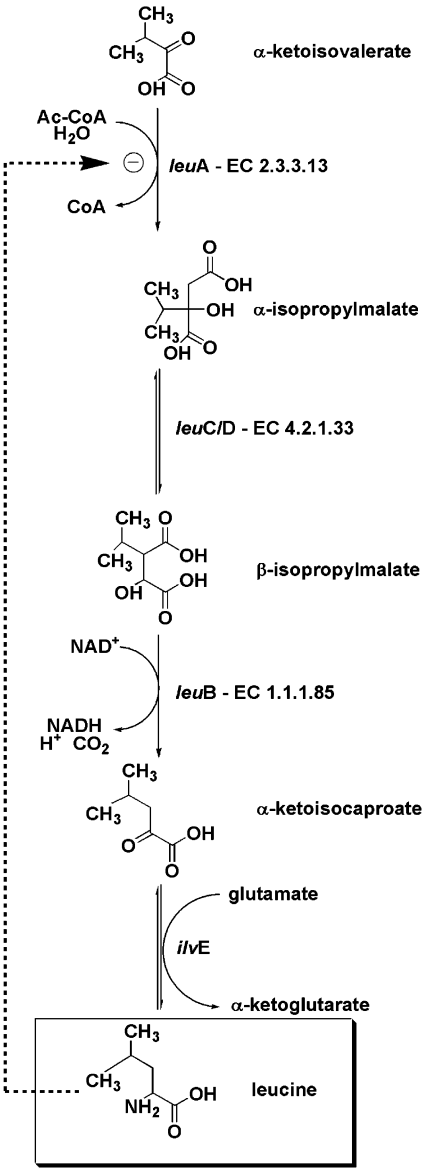

condensation reaction using quite different catalytic mechanisms. MS from both yeast and *M. tuberculosis* use a Mg^{2+} ion (*9*, *10*) to bind and polarize the carbonyl group of glyoxylate, while CS does not use a divalent metal but rather a pair of histidine residues to polarize the carbonyl group of oxaloacetate. In addition, CS from different organisms can display quite different pH dependences, with the *Thermoplasma acidophilum* CS reaction being independent of pH and the pig heart CS reaction being dependent upon two ionizable enzyme groups (*11*).

IPMS from *Salmonella enterica* serovar *Typhimurium* (*12*−*15*), *Alcaligenes eutrophus* H16 (*16*−*18*), *Neurospora* (*19*), and *Saccharomyces* (*20*) have been partially characterized. The common features of most α-IPM synthases are a requirement for monovalent cations for maximal activity, feedback inhibition by L-leucine, and narrow substrate specificity for analogues of α-KIV. In contrast, there are many differences revealed by these studies, including the effects of divalent metals, inhibition by some α-keto acids, feedback regulation, and allosteric properties. Chanchaem and Palittapongarnpim have cloned, expressed, and purified active *Mt*IPMS, but no rigorous kinetic studies were performed (*21*). Recently, Koon et al. solved the three-dimensional crystal structure of IPMS from *M. tuberculosis* with Zn^{2+} and α-KIV bound at the active site (*22*). The insertion of two residues of one monomer into the active site of the other in the dimeric enzyme suggests how regulation by L-leucine may be achieved (*22*). Our own studies have revealed an absolute dependence for a monovalent cation for activity, and potassium appears to be the physiologically relevant monovalent ion. Additionally, the monovalent cation is required for the binding of and activation of catalysis by a divalent metal that is used to coordinate the carbonyl and carboxyl oxygens of α-KIV (*25*).

This paper describes the detailed biochemical characterization of the recombinant IPMS from *M. tuberculosis* $H37R_v$. Using a combination of steady-state kinetics, primary deuterium and solvent kinetic isotope effects (KIEs), isotopic labeling, and ^1H nuclear magnetic resonance (NMR) spectroscopy, the following questions were addressed. (i) What is the substrate specificity for α-keto acids and acyl-CoA analogues? (ii) What is the kinetic mechanism of *Mt*IPMS? (iii) Does acid/base chemistry play an important role in catalysis? (iv) Does the enzyme hydrolyze acyl-CoA analogues? (v) What is the rate-limiting step in the reaction? (vi) What is the chemical mechanism used for intermediate cleavage?

MATERIALS AND METHODS

Materials. (*R*)-Hydroxyisovalerate was obtained from Fluka. α-Keto acids, acyl-CoAs, buffers, and all other chemicals were obtained from Sigma, Aldrich, or Fisher. Nickel−NTA resin was from Novagen. Chromatographic columns and resins were obtained from Pharmacia. Chelex 100 was purchased from Bio-Rad.

General Methods. The protein concentration was measured using the bicinchoninic acid method (Pierce), using bovine serum albumin as a standard. Protein electrophoresis was performed using the Phast System (Pharmacia) and 10−15% sodium dodecyl sulfate−polyacrylamide gel electrophoresis (SDS−PAGE) gradient PhastGels. All spectrophotometric assays were performed using a UVIKON XL UV-vis spectrophotometer equipped with a circulating water bath and thermospacers. All experiments analyzed using Lineweaver−Burke plots were performed in duplicate or triplicate when the measured parameters were greater than 10% different in duplicate experiments. NMR spectroscopy experiments were performed on a Bruker DRX300 NMR spectrometer at 25 °C (AECOM Structural NMR Resource). Cloning of the *leu*A gene (Rv3710) and expression and purification of *Mt*IPMS are described elsewhere (*4*).

Characterization of IPMS. The monomer molecular mass was estimated by SDS−PAGE. Protein samples were analyzed by electrospray ionization/mass spectrometry (Laboratory of Mass Spectrometry and Proteomics, Albert Einstein College of Medicine) for accurate determination of the monomer mass.

Oligomeric State. Analytical gel-filtration experiments were performed with a Superose 12 column (Pharmacia) in 20 mM triethanolamine (TEA) at pH 7.8 containing 100 mM KCl at a flow rate of 0.2 mL/min. Dynamic light scattering was measured with a DynaPro MS/X dynamic light-scattering instrument (Protein Solutions) with samples of

*Mt*IPMS at 10 mg/mL in 20 mM TEA at pH 7.8. Sedimentation velocity experiments were performed in a Beckman Optima XL-1 analytical centrifuge at 25 °C and a rotor speed of 35 000 rpm using an An-Ti 60 rotor. Sedimentation boundaries were followed at 280 nm using the absorption optics. The samples were loaded into double-sector centrifuge cells and equilibrated at 25 °C for 15−30 min prior to initiating centrifugation. The sedimentation and diffusion coefficients were determined using SVEDBERG version 6.39 (*23*), using a $\bar{v} = 0.7173$ calculated from the amino acid composition. These parameters were normalized to the standard conditions of 20 °C using SEDNTERP version 1.08.

Measurement of Enzymatic Activity. Initial velocities for the forward reaction of IPMS were determined using 4,4′-dithiodipyridine (DTP) to detect the formation of coenzyme A (CoA) at 324 nm ($\epsilon = 19\,800$ M^{-1} cm^{-1}) at 25 °C (*24*). A typical reaction mix contained 50 mM *N*-[2-hydroxyethyl]-piperazine-*N*′-[2-ethanesulfonic acid] (HEPES) at pH 7.5, 20 mM KCl, 20 mM $MgCl_2$, 100 μM DTP, 1 mM AcCoA, and 0.5 mM α-KIV. Reactions were initiated by the addition of the enzyme, typically a 20 nM final concentration. Potassium and magnesium were included because they are required for maximal activity (*25*). An alternative assay monitored the decrease in absorbance at 232 nm because of the hydrolysis of the thioester of AcCoA ($\Delta\epsilon = 4500$ M^{-1} cm^{-1}), using either phosphate or tris(hydroxymethyl)aminomethane (Tris) buffers (*26*).

Product Analysis by ^1H NMR. The reaction of *Mt*IPMS with AcCoA and α-KIV was followed by ^1H NMR. Reaction mixtures consisted of 50 mM potassium phosphate buffer at pH 7.0, 12 mM $MgCl_2$, 1.1 mM α-KIV, 1 mM AcCoA, and 100 μg of *Mt*IPMS. Reactions containing propionyl-CoA and α-KIV were performed in a similar manner.

Preparation of [$^2H_3$-Methyl]AcCoA. [$^2H_3$-Methyl]AcCoA was prepared by S-acetylation of CoA using deuterated acetic anhydride (Aldrich). A typical acetylation reaction contained 100 mM TEA at pH 7.8, 40 mM [$^2H_3$-methyl]acetic anhydride, and 20 mM CoA in 1 mL of 50% ethanol. The reaction was monitored using DTP, and the reaction was complete in 10 min at 37 °C. Reaction mixtures were stored at −20 °C, and the exact concentration of [$^2H_3$-methyl]-AcCoA was determined spectrophotometrically (*26*), using the adenine ring absorbance at 260 nm ($\epsilon = 16\,400$ M^{-1} cm^{-1}) and the thioester bond absorbance at 232 nm ($\epsilon = 8700$ M^{-1} cm^{-1}). The values obtained agreed to ±1%, indicating the stability of AcCoA under these conditions. The extent of deuteration of [$^2H_3$-methyl]AcCoA was determined by ^1H NMR.

pH Studies. The pH dependence of $V/K_{\alpha-KIV}$ (k_{cat}/K_m) was determined by varying the concentration of α-KIV at a fixed, saturating concentration of AcCoA. The pH dependence of V/K_{AcCoA} (k_{cat}/K_m) and V (k_{cat}) was determined by varying the concentration of AcCoA at a fixed, saturating concentration of α-KIV (*27*). The following buffers were used at the indicated pH ranges: 2-(*N*-morpholino)ethanesulfonic acid (MES), pH 6.50; piperazine-*N*,*N*′-bis[2-ethanesulfonic acid] (PIPES), pH 6.38−7.15; HEPES, pH 7.11−7.87; *N*-tris-[hydroxymethyl]methyl-2-aminopropanesulfonic acid (TAPS), pH 8.05−8.79; and 2-(*N*-cyclohexylamino)ethanesulfonic acid (CHES), pH 8.97. Experiments were performed with Good buffers, which have low metal-binding capabilities, using overlapping pH values (*27*, *28*).

Primary Deuterium and Solvent Isotope Effects. Isotope effects were determined in 100 mM TAPS at pH 8.3 and saturating concentrations of Mg^{2+} and K^+. Primary deuterium KIEs on V and V/K_{AcCoA} were determined using [$^1H_3$-methyl]- and [$^2H_3$-methyl]AcCoA in the presence of saturating concentrations of either α-KIV or pyruvate (PY). Solvent KIEs on V and V/K_{AcCoA} were determined in water or 80% deuterium oxide, in the presence of saturating concentrations of either α-KIV or PY at pH 8.3. The proton inventory on the V_{max} was performed by varying the atom fraction of deuterium oxide from 0 to 0.8 in increments of 0.2, in quadruplicate in the presence of saturating concentrations of substrates.

Enolization and Hydrolysis of AcCoA. Enzyme-catalyzed enolization of AcCoA was assessed by ^1H NMR in D_2O. The intensity of the peak corresponding to the α-methyl protons from AcCoA was measured as a function of time. Enzyme-catalyzed hydrolysis of AcCoA was also determined by ^1H NMR because the methyl proton resonances of AcCoA and acetic acid appear at different frequencies. Typical incubation mixtures contained 100 mM NaH_2PO_4 at pH 7.0, 10 mM KCl, 2 mM AcCoA, and 11.6 μM IPMS in 600 μL of D_2O. The effect of Mg^{2+} was probed by adding 12 mM $MgCl_2$ to the reaction mixture. Enolization in the presence of either (*R*)- or (*S*)-α-hydroxyisovalerate (α-HIV) was tested at concentrations of the alcohols at 3.5 mM. The intensity of the peaks were normalized relative to the peaks from the gem dimethyl groups of the pantetheine moiety of CoA.

Mechanism of Hydrolysis by the ^{18}O-Isotope-Induced Shift on the ^{13}C-NMR Signal. To probe the possible existence of an anhydride intermediate during the hydrolysis of the α-isopropylmalyl-CoA thioester intermediate, we measured the ^{18}O-induced isotope shifts of the ^{13}C carbon resonances of the product, α-IPM (*29*, *30*). The reaction mixture contained 100 mM NaH_2PO_4 at pH 7.0, 8 mM KCl, 12 mM $MgCl_2$, 20 mM AcCoA, 15 mM α-KIV, and 5 μM IPMS in 1 mL (70% v/v, $H_2{}^{18}O$). The reaction was allowed to proceed at 37 °C for 120 min. The enzyme was removed by ultrafiltration, and the ultrafiltrate was lyophilized. The lyophilized powder was suspended in 300 μL of D_2O, and the ^{13}C spectrum was determined using ^1H-decoupled ^{13}C NMR, averaging 60 000 scans.

Data Analysis. Kinetic data were fitted using the nonlinear, least-squares, curve-fitting programs of SigmaPlot 2000 for Windows, version 6.00. Individual saturation curves were fitted to

$$\nu = VA/(A + K) \quad (1)$$

where V is the maximal velocity, A is the substrate concentration, and K is the Michaelis constant for the substrate (K_m). Individual saturating curves showing linear substrate inhibition were fitted to

$$\nu = VA/(K + A + (A^2/K_i)) \quad (2)$$

where K_i is the apparent inhibition constant for substrate A. Data showing an intersecting initial velocity pattern on double-reciprocal plots were fitted to

$$\nu = VAB/(K_{ia}K_B + K_AB + K_BA + AB) \quad (3)$$

where A and B are the concentrations of the substrates and

K_A and K_B are the Michaelis constants. Inhibition data showing linear, competitive or noncompetitive patterns in double-reciprocal plots were fitted to eqs 4 and 5, respectively

$$\nu = VA/[K(1 + I/K_{is}) + A] \quad (4)$$

$$\nu = VA/[K(1 + I/K_{is}) + A(1 + I/K_{ii})] \quad (5)$$

where I is the inhibitor concentration and K_{is} and K_{ii} are the slope and intercept inhibition constants, respectively. Inhibition data, performed under saturating concentrations of substrates and variable concentrations of inhibitors, were fitted to

$$\nu = \nu_0/[1 + (I/IC_{50})^{n_H}] \quad (6)$$

where υ is the rate in the presence of the inhibitor at concentration I, υ_0 is the rate without the inhibitor, IC_{50} is the concentration of the inhibitor that gives 50% inhibition, and n_H is the Hill coefficient. pH profile data were fitted to eq 7 for two nonresolvable acidic ionizable groups, eq 8 for two acidic nonresolvable and one basic ionizable group, and eq 9 for two acidic nonresolvable and two basic nonresolvable ionizable groups

$$\nu = C/(1 + H^2/K_a^2) \quad (7)$$

$$\nu = C/[1 + (H^2/K_a^2) + K_b/H] \quad (8)$$

$$\nu = C/[1 + (H^2/K_a^2) + (K_b^2/H^2)] \quad (9)$$

where C is the pH-independent plateau value, H is the hydrogen ion concentration, and K_a and K_b are the respective acidic and basic pK_a constants for the ionizable groups. Primary deuterium and solvent isotope effects were fitted to eqs 10, 11, and 12, for isotope effects on V only, V/K only, or both V and V/K, respectively

$$\nu = VA/[K + A(1 + F_iE_V)] \quad (10)$$

$$\nu = VA/[K(1 + F_iE_{V/K}) + A] \quad (11)$$

$$\nu = VA/[K(1 + F_iE_{V/K}) + A(1 + F_iE_V)] \quad (12)$$

where F_i is the fraction of the isotopic label and E_V and $E_{V/K}$ are the isotope effects minus one on V and V/K, respectively. The linear proton inventory on V_{max} was fitted to

$$V_n = V_o[1 - n + n(k_D/k_H)] \quad (13)$$

where n is the atom fraction of deuterium in the mixed isotopic solvent, V_n is the velocity in the solvent with the atom fraction of deuterium n, V_o is the velocity in H_2O, and k_D/k_H is the isotope effect. Errors were propagated as described in Skoog and West for indeterminate errors (*31*).

RESULTS

General Properties of MtIPMS. Gel filtration of the homogeneous protein over a Superose 12 column generated a single peak that eluted at the position of the dimer in the presence of 100 mM KCl (data not shown). Dynamic light scattering revealed that, in the absence or presence of 100 mM KCl, the protein is a dimer (data not shown). The sedimentation and diffusion coefficients were determined for *Mt*IPMS at protein concentrations ranging from 2.4 to 9.3 μM in 40 mM TEA at pH 7.8 containing 8 mM KCl and 12 mM $MgCl_2$, in the absence or presence of L-leucine. The sedimentation boundaries are well-described by a single component; S and D linearly decreased with an increasing protein concentration, consistent with the protein behaving as a noninteracting monodisperse particle (data not shown). Extrapolation to infinite dilution yields values of $S°_{20,w}$ of 8.6 ± 0.3 and 8.7 ± 0.3 S, respectively, and $D°_{20,w}$ of 7.8 ± 0.6 and 9.2 ± 0.8 F, respectively. The values of S and D calculated (*32*) from the crystal structure of the *Mt*IPMS dimer (*22*) are 8.97 and 5.08 F, respectively.

Table 1: Steady-State Kinetic Parameters for *Mt*IPMS[a]

fixed substrate	variable substrate	k_{cat} (s^{-1})	K_m (μM)	k_{cat}/K_m (s^{-1} M^{-1}) ($\times 10^{-2}$)
AcCoA	α-KIV	3.5 ± 0.1	12 ± 1	34 000 ± 260
AcCoA	α-KV	7.0 ± 1.3	410 ± 180	5900 ± 80
AcCoA	α-KB	10.7 ± 0.4	860 ± 160	8000 ± 25
AcCoA	PY	6.1 ± 0.5	9500 ± 1680	16 ± 1
α-KIV	AcCoA	2.1 ± 0.1	136 ± 5	150 ± 9
α-KV	AcCoA	5.0 ± 0.2	279 ± 31	180 ± 20
α-KB	AcCoA	7.6 ± 0.1	57 ± 2	1300 ± 49
PY	AcCoA[b]	4.5 ± 0.3	74 ± 13	610 ± 120

[a] At pH 7.4 and 25 °C. The following concentrations of fixed cosubstrate were used: 1 mM AcCoA, 250 μM α-KIV, 4 mM α-KV, 10 mM α-KB, and 100 mM PY. [b] Saturation curves displaying apparent linear substrate inhibition were fitted to eq 2. The K_i for α-KV at a fixed saturating concentration of AcCoA was 10.1 ± 4.4 mM, and the K_i for AcCoA in the presence of a fixed saturating concentration of PY was 4.0 ± 1.3 mM.

Initial Velocity Studies. To characterize the kinetic mechanism, we performed initial velocity studies. The intersecting initial velocity pattern obtained by varying the concentration of α-KIV at fixed variable concentrations of AcCoA (see the Supporting Information) is consistent with a sequential bi-bi kinetic mechanism (*33*).

Substrate Specificity. Kinetic parameters for α-keto acids and AcCoA are summarized in Table 1. No activity was detected up to a 5 mM concentration of the following analogues: glyoxalate, α-ketoisocaproate, α-keto-β-methyl-*n*-valerate, α-ketoglutarate, phenylpyruvate, and phenylglyoxalate. The apparent substrate inhibition observed with some α-keto acids (see the Supporting Information) will be discussed below. The α-keto acids that are substrates for *Mt*IPMS are α-KIV, PY, α-ketovalerate (α-KV), and α-ketobutyrate (α-KB). The data presented in Figure 1A reveals that there is no "uncoupled" hydrolysis of AcCoA in the presence of α-KIV and that the reaction rate measured in steady-state experiments is entirely due to the hydrolysis of the initially formed condensation product, α-isopropylmalyl-CoA. Using propionyl-CoA, a very small quantity of the condensation product of α-KIV and propionyl-CoA is observed by ^{1}H NMR (Figure 1B). However, greater than 95% of the steady-state rate observed with propionyl-CoA is due to hydrolysis. The rate of hydrolysis of propionyl-CoA is much slower than the rate of condensation and hydrolysis observed using AcCoA and α-KIV, which is complete in a few minutes under these conditions. Measurements of the rates of hydrolysis of AcCoA, propiony-CoA, and crotonyl-CoA in the absence of α-KIV, under steady-

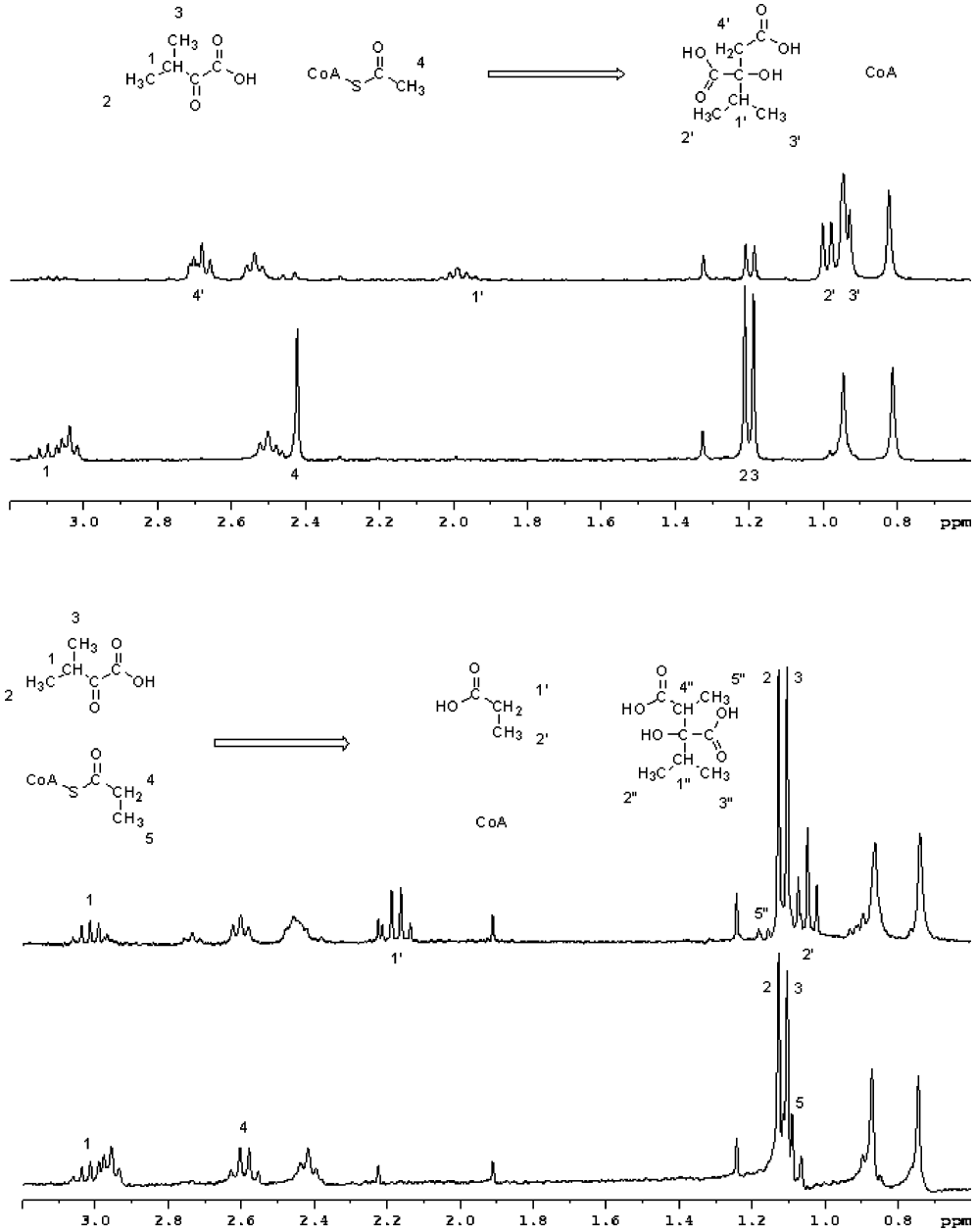

FIGURE 1: ^{1}H-NMR analysis of the reaction of *Mt*IPMS. (A) Region of spectral interest of the reaction of *Mt*IPMS with AcCoA and α-KIV. Reaction mixture without enzyme (bottom spectrum) and reaction after reaching completion (top spectrum). (B) Region of interest of the spectra of the reaction of *Mt*IPMS with propionyl-CoA and α-KIV. Reaction mixture without enzyme (bottom spectrum) and reaction after reaching completion (top spectra). Although data were recorded throughout the experiments, only the last spectrum is shown in each case.

Table 2: Steady-State Kinetic Parameters for the α-Keto Acid-Independent Hydrolysis of Acyl-CoA Analogues Catalyzed by *Mt*IPMS[a]

	without added $MgCl_2$			with added $MgCl_2$		
	K_m (μM)	k_{cat} (s^{-1})	k_{cat}/K_m ($s^{-1}\ M^{-1}$)	K_m (μM)	k_{cat} (s^{-1})	k_{cat}/K_m ($s^{-1}\ M^{-1}$)
acetyl-CoA	370 ± 40	$(6 \pm 0.3) \times 10^{-2}$	150 ± 19	160 ± 29	$(3 \pm 0.2) \times 10^{-2}$	170 ± 36
propionyl-CoA	220 ± 40	$(4 \pm 0.3) \times 10^{-2}$	190 ± 36	ND[b]	ND	
crotonyl-CoA	50 ± 3	$(5 \pm 0.2) \times 10^{-2}$	940 ± 72	95 ± 15	$(4 \pm 0.2) \times 10^{-2}$	400 ± 70

[a] Performed at 25 °C and pH 7.4. [b] ND = not determined.

state conditions, indicate that *Mt*IPMS very slowly hydrolyzes acyl-CoA analogues (Table 2 and data not shown). These results confirm that AcCoA is the only acyl-CoA analogue accepted in the condensation reaction by *Mt*IPMS.

Product and Dead-End Inhibition Studies. Because of the nature of our assay that precludes the use of any compound with a free thiol (e.g., CoA) and the high K_m for AcCoA, we did not attempt to use CoA as a product inhibitor to study the order of substrate binding. Product inhibition studies with α-IPM and dead-end inhibition studies with (*S*)-α-HIV (α-KIV analogue) and dethio-CoA (CoA analogue) were performed, and the results are summarized in Table 3. The

Table 3: Product and Dead-End Inhibition Patterns for *Mt*IPMS[a]

varied substrate	inhibitor	concentration of the cosubstrate	pattern[b]	K_{is} (mM)	K_{ii} (mM)
AcCoA	α-IPM	sat α-KIV	NI[c]		
AcCoA	α-IPM	5× K_m α-KIV	NC	0.02 ± 0.03	0.07 ± 0.04
α-KIV	α-IPM	sat AcCoA	C	0.20 ± 0.15	
α-KIV	(*S*)-α-HIV	sat AcCoA	NC	1.7 ± 0.6	20.7 ± 5.3
α-KIV	dethio-CoA	sat AcCoA	NC	2.4 ± 0.6	1.8 ± 0.2
AcCoA	dethio-CoA	sat α-KIV	C	1.06 ± 0.04	

[a] At pH 7.4, 25 °C, 20 mM KCl, and 20 mM $MgCl_2$. The concentration of cosubstrates was held fixed and saturating (500 μM α-KIV and 1 mM AcCoA), unless otherwise stated. [b] C = competitive, and NC = noncompetitive. [c] NI = no inhibition.

competitive patterns obtained with α-IPM versus α-KIV and dethio-CoA versus AcCoA indicate a random bi-bi kinetic mechanism. Further support for the random nature of substrate binding comes from the apparent linear substrate inhibition observed under some experimental conditions (see Table 1 and the Supporting Information). These patterns are a hallmark of nonrapid equilibrium random bi-bi kinetic mechanisms where there is a preferred route to the ternary complex (*34*, *35*).

Enolization and Hydrolysis of AcCoA. To gain information about the chemical mechanism of *Mt*IPMS, we examined the enzyme-catalyzed exchange of the α-methyl protons of AcCoA in D_2O in the absence of α-KIV using ^{1}H-NMR spectroscopy. Figure 2A shows a representative stack plot of ^{1}H-NMR spectra over the course of the reaction. The singlet at 2.45 ppm corresponds to the three methyl hydrogens from the acetyl group of AcCoA; the singlet at 1.95 ppm arises from the methyl hydrogens of acetate; and the singlet at 0.95 ppm corresponds to the pantetheine gem dimethyl hydrogens used as an internal calibration. Figure 2B is a plot of the corrected intensities of the peaks shown in Figure 2A versus time. The excellent correspondence between the disappearance of the AcCoA peak and the appearance of an acetate peak indicates that *Mt*IPMS does not catalyze the exchange of the α-methyl protons of AcCoA with solvent at any significant rate but does slowly hydrolyze AcCoA. This rate is $(3.0 \pm 0.2) \times 10^{-2}$ s^{-1} in the presence of saturating mono- and divalent metals (Table 2). The presence of $MgCl_2$ or product analogues, like (*R*)- or (*S*)-α-HIV, did not have any effect on the rates of hydrolysis or enolization of AcCoA (data not shown).

pH Studies. To probe the role of general acid/base chemistry in the mechanism of *Mt*IPMS, we determined the pH dependence of k_{cat} and k_{cat}/K_m for both substrates, in the region of 6.00 ≤ pH ≤ 9.00 (Figure 3). The k_{cat} profile displays a sharp decrease at low pH, with a slope of two. A fit of the data to eq 7, for two nonresolvable[2] ionizable basic groups, provided estimates of the pK_a values of 6.7 ± 0.1, suggesting that there are two active-site bases that are essential for chemistry. The $k_{cat}/K_{\alpha-KIV}$ profile is bell-shaped, with a slope of 2 on the acidic side and a slope of 1 on the basic side. A fit of the data to eq 8 provided estimates of the pK_a values of the two ionizable groups on the acidic side of 7.0 ± 0.1 and the basic ionizable group of 8.6 ± 0.3. This group may correspond to Arg80 that is observed in the crystal structure to be within hydrogen-bonding distance of the carbonyl group of the metal-bound α-KIV. The k_{cat}/K_{AcCoA} profile is also bell-shaped, with slopes of two on both the acidic and basic limbs. The basic residues exhibit pK_a values of 6.5 ± 0.1, and the acidic residues exhibit pK_a values of 8.5 ± 0.2 (eq 9). The bases seen in both k_{cat}/K_m profiles are most likely the same seen in the k_{cat} profile, and their slight shift from the values observed in the k_{cat} profiles is probably due to the stickiness of the substrates.[3] The pK_a of the enzymic acidic residues are most likely shifted outward because of the same reason. The groups seen at high pH values in the k_{cat}/K_m profiles are involved in substrate binding (*27*) and not catalysis, but we have no structural information with which to assign these groups to the corresponding amino acids.

Primary Deuterium Isotope Effects. To define the rate-limiting step and characterize the chemical mechanism, we performed isotope effect experiments using [$^1H_3$-methyl]- and [$^2H_3$-methyl]AcCoA.[4] No KIE was observed at fixed saturating concentrations of α-KIV and variable concentrations of [$^1H_3$-methyl]- or [$^2H_3$-methyl]AcCoA at pH values of 6.3, 7.2, and 9.0. Substitution of α-KIV with α-KB or PY, which have K_m values 70- and 800-fold higher than α-KIV, respectively, yielded similar results at pH 7.2. Similar results were obtained using saturating concentrations of [$^1H_3$-methyl]- or [$^2H_3$-methyl]AcCoA and varying α-KIV (data not shown). The absence of any measurable primary deuterium KIE using deuterated AcCoA, at various pH values and with different substrates, strongly suggests that deprotonation and enolization of AcCoA are not the rate-determining steps in the *Mt*IPMS reaction.

Solvent Isotope Effects. Solvent isotope effects were performed at pH 8.3 using 100 mM TAPS buffer. Using

[2] pH profile data showing slopes >1 or < −1 are usually fitted to equations such as $v = C/[(1 + H/K_{a_1}) + (1 + H/K_{a_2}) + (K_{b_1}/H) + (K_{b_2}/H)]$, which describe the pH dependence of a rate constant on the ionization of two different conjugated acids and two different conjugated bases. During the analysis of our data, it became clear that this equation did not fit our data well (e.g., very large standard error was associated with the *K* values). This might be due to the two p*K* values being very close one to another (e.g., nonresolvable) or that the addition of the extra variables requires many additional data points at lower and higher pH values, which are difficult to obtain with high accuracy, to increase the precision of the fit.

[3] The pK_a values seen in k_{cat}/K_m profiles but not in k_{cat} profiles of sticky substrates are usually displaced outward by 0.3−0.5 pH units, to lower pH values when protonation decreases activity and to higher pH values when deprotonation decreases activity (*26*).

[4] Using UV and ^{1}H-NMR spectroscopy, we were able to determine that greater than 99% of CoA was converted to [$^2H_3$-methyl]AcCoA, under the experimental conditions described (data not shown). MALDI−TOF analysis indicates that 9.6 ± 0.4% of the product was bis-acetylated (data not shown). In the presence of α-KIV, the rates observed using [$^2H_3$-methyl]AcCoA or commercial [$^1H_3$-methyl]AcCoA were identical, under a variety of conditions, suggesting that the 9.6% of the [$^2H_3$-methyl]AcCoA that was bis-acetylated does not have any effect that invalidates our conclusions.

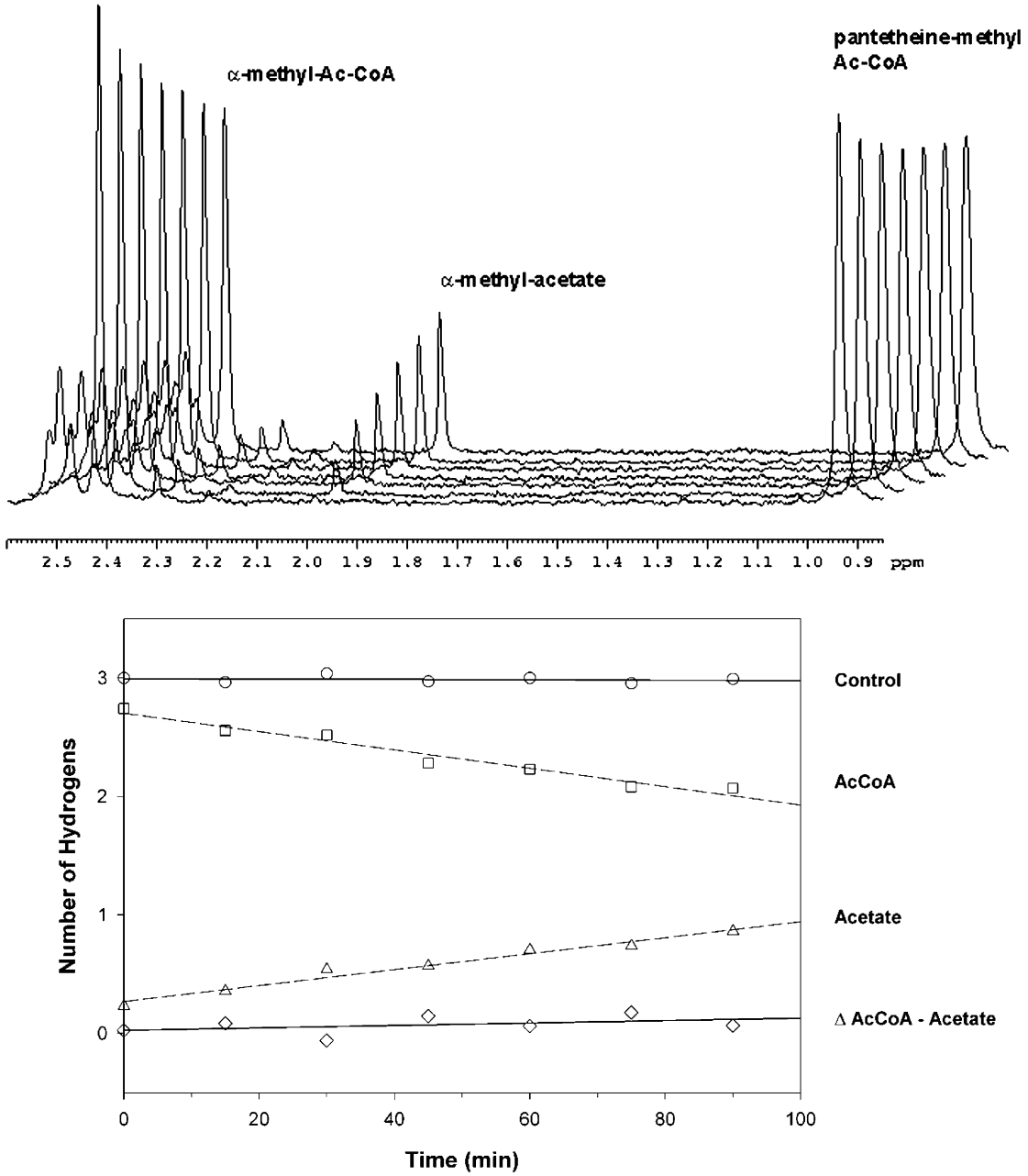

FIGURE 2: *Mt*IPMS-catalyzed enolization and hydrolysis of AcCoA probed by ^{1}H NMR. (A) Stack plot of the region of interest from the ^{1}H-NMR spectra of the reaction of *Mt*IPMS with AcCoA. The spectra were recorded at 0, 15, 30, 45, 60, 75, and 90 min. The peak at 2.3 ppm corresponds to the protons of the acetyl group of the AcCoA; the peak at 1.95 corresponds to the protons of the free acetate; and the peak at 0.94 ppm corresponds to the protons of the gem dimethyl groups of the pantetheine moiety of AcCoA, used as an internal control. (B) Plot of the corrected intensity of each peak versus time. The control peak is represented by ○; AcCoA protons are represented by □; the acetate peak is represented by △; and the difference between the acetyl and acetate groups, which correspond to the exchange or enolization, are represented by ◇.

α-KIV as the α-keto acid substrate, small solvent isotope effects (0.9−1.2) were observed that are unlikely to be statistically significant. Using PY as a substrate, we were able to measure larger, normal solvent isotope effects[5] (Table 4). The proton inventory on V_{max}, using saturating concentrations of AcCoA and PY, was linear. The linear proton inventory indicates that there is only one proton being transferred in the transition state for hydrolysis. These results support the idea that, although with the natural substrate, hydrolysis is not rate-limiting, using less sticky substrates, the hydrolytic step becomes partially rate-limiting.

Hydrolysis of α*-Isopropylmalyl-CoA.* To determine the mechanism used by *Mt*IPMS to hydrolyze the α-isopropylmalyl-CoA intermediate (inset of Figure 4), we used an ^{18}O-labeling strategy and measured the ^{18}O-induced shift on the ^{13}C-NMR resonance for the product. Figure 4 shows the downfield carboxylate region of the ^{13}C-NMR spectra of the α-IPM product generated in 72% $H_2{}^{18}O$. The peak corresponding to the C1 carboxylate of α-IPM (182.6 ppm) is a singlet, while the C4 carboxylate resonance (180.3 ppm) is

[5] The observation of normal solvent isotope effects for the reaction catalyzed by *Mt*IPMS is inconsistent with the prediction, on the basis of the crystal structure, that a metal-bound water molecule is involved in the hydrolytic step (*22*). Metal-bound water molecules have fractionation factors smaller than 1 and therefore will give rise to inverse solvent isotope effects (*42*).

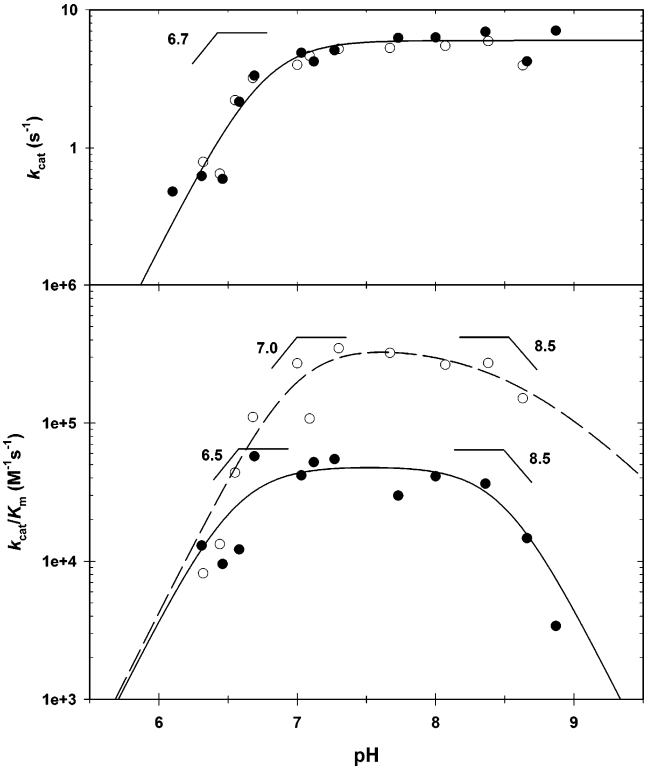

FIGURE 3: pH profiles of the *Mt*IPMS reaction. The k_{cat} and K_m values were determined at each pH by varying the concentration of one substrate at a fixed saturating concentration of the other substrate and saturating concentrations of K^+ and Mg^{2+}. The AcCoA data are represented by ●, and the best fit of the data is represented by —. The α-KIV data is represented by ○, and the best fit of the data is represented by - - -.

Table 4: Solvent Isotope Effects for *Mt*IPMS[a]

solvent isotope effects			
fixed substrate	variable substrate	^{D_2O}V	$^{D_2O}V/K$
PY	AcCoA	2.0 ± 0.2	1
AcCoA	PY	1.8 ± 0.2	2.2 ± 0.5

[a] Solvent isotope effects were determined in 100% H_2O or 80% D_2O, at pH 8.3 and 25 °C.

composed of two singlets, one corresponding to the carboxylate containing ^{18}O (ca. 70%) and the other corresponding to the ^{16}O-containing carboxylate. The isotope-induced shift on the ^{13}C resonance expected for a carboxylate-containing ^{18}O is about 0.035 ppm (*36*, *37*), and we observed a 0.029 ppm isotope-induced shift. This result strongly suggests that hydrolysis of the α-isopropylmalyl-CoA thioester is unlikely to occur via intramolecular attack by the distal carboxylate on the thioester to generate the anhydride and CoA in solution. However, the formation of an intramolecular anhydride and its regiospecific hydrolysis on the enzyme cannot be formally ruled out by this result.

DISCUSSION

General Properties. Gel filtration, dynamic light scattering, and sedimentation velocity experiments demonstrate that *Mt*IPMS is a dimer in solution and this oligomeric state is not influenced by the K^+ concentration, as is observed for bacterial citrate synthases (*38*). In addition, the sedimentation velocity studies show that L-leucine has no effect, within experimental error, on the oligomerization state of *Mt*IPMS at the protein concentrations analyzed. The correspondence of the measured coefficients suggests that *Mt*IPMS is a stable dimer in solution. The difference between the measured and calculated diffusion coefficient is intriguing in light of the observation from the *Mt*IPMS structure that *Mt*IPMS forms an extended dimer (*22*). The sedimentation data suggest a more compact arrangement of the regulatory and catalytic domains in solution than is observed in the crystal.

Substrate Specificity. The α-keto acid specificity of *Mt*IPMS is very similar to what was reported for the IPMS of yeast, *Salmonella*, *Alcaligenes*, and *Neurospora* (*14*, *16*, *19*, *20*). Only small α-keto acids can be accommodated in the active site, in agreement with the small size and hydrophobicity of the α-KIV-binding site observed in the crystal structure (*22*).

The broad acyl-CoA specificity reported for some IPMS enzymes from other organisms should be viewed cautiously. The lack of a rigorous analysis of the products of the reaction and the nature of the spectrophotometric assay used in these studies suggest that previous studies were incapable of distinguishing between *bona fide* condensation of the acyl-CoA substrate and simple hydrolysis uncoupled from condensation (*14*, *16*, *19*, *20*). In addition, the rates of hydrolysis of these acyl-CoA analogues were not performed in the absence of α-KIV. Our data, specifically the ^1H-NMR analysis of the reaction of AcCoA or propionyl-CoA with α-KIV, indicate that propionyl-CoA is a very poor substrate and that the rate observed in the presence of α-KIV is due to the hydrolysis of propionyl-CoA rather than its condensation and hydrolysis (Figure 2B). Kinetic evidence comparing the rates of hydrolysis of propionyl-CoA and crotonyl-CoA in the absence or presence of α-KIV argues that *Mt*IPMS cannot use CoA-linked acyl chains longer than two carbons. Inspection of the structure confirms that there is not enough room to accommodate a longer acyl group in the active site (*22*). In summary, *Mt*IPMS has a very narrow acyl donor substrate specificity, using only AcCoA as the substrate.

Kinetic Mechanism. The intersecting initial velocity pattern obtained indicates that *Mt*IPMS requires the formation of a ternary complex before chemistry can take place. The patterns obtained using product and dead-end inhibitors are most consistent with a random bi-bi kinetic mechanism (Scheme 2), with α-IPM being a competitive inhibitor versus α-KIV and dethio-CoA being a competitive inhibitor versus AcCoA. The two noncompetitive patterns observed (Table 3) are also indicative of a random mechanism with the formation of the abortive E/α-KIV/CoA and E/α-IPM/AcCoA complexes (Scheme 2).

Further indications of random substrate binding comes from the nonhyperbolic kinetics observed using variable amounts of α-KV at saturating concentrations of AcCoA, showing concave downward curvature on a double-reciprocal plot (see the Supporting Information), and using variable concentrations of AcCoA in the presence of saturating concentrations of PY, displaying concave upward curvature on the double-reciprocal plot (see the Supporting Information). In random but not ordered mechanisms, upward curvature in a double-reciprocal plot indicates that the rate of the chemical steps is greater than the rate of substrate release (*39*, *40*). These substrate inhibition patterns are commonly found in nonrapid equilibrium random systems,

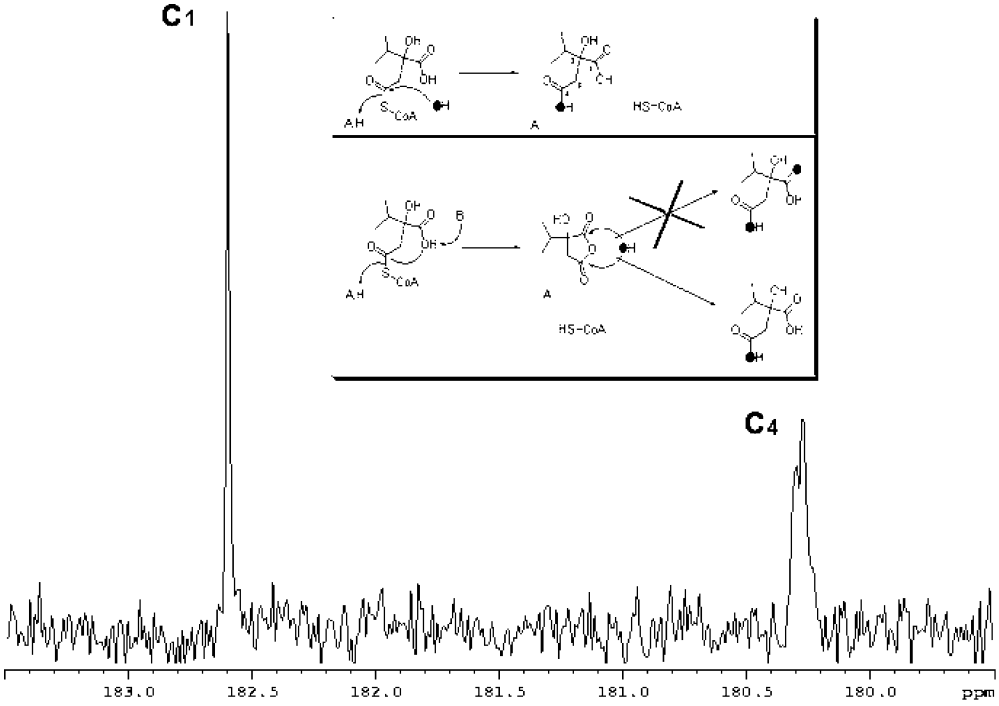

FIGURE 4: ^{18}O labeling of α-isopropylmalyl-CoA hydrolysis. Region of interest of the ^{1}H-decoupled ^{13}C spectra showing the resonances of the C1 and C4 atoms of α-IPM and the unique ^{18}O isotope-induced shift on the C4 carboxylate of α-IPM. Inset shows the scheme for the possible mechanisms for hydrolysis of α-isopropylmalyl-CoA and the labeling patterns generated. The top panel represents the direct hydrolysis, where ^{18}O is represented by ●. The bottom panel represents the two mechanisms that could promote hydrolysis of the intramolecular anhydride formed by the attack of C1 on the C4 thioester. The upper pathway represents a nonregioselective hydrolysis (in solution), and the lower pathway represents a regioselective hydrolysis (at the active site).

Scheme 2

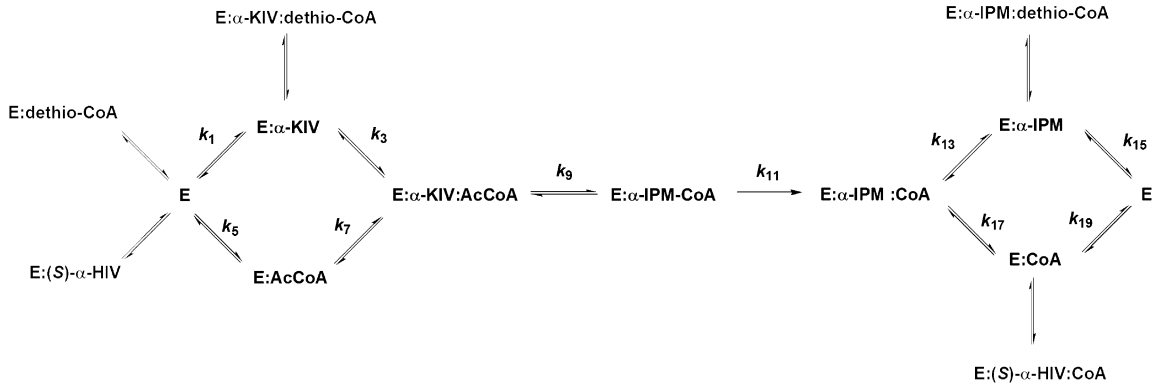

where there is a preferred pathway to the ternary complex (*34*, *35*, *39*−*41*). The rapid equilibrium assumption is not valid for *Mt*IPMS because the k_{cat}/K_m values for all of the α-keto acid substrates are much lower than one would expect for a diffusion-controlled reaction, around 10^9 s^{-1} M^{-1} (*42*).

A nonunitary *V*/*K* isotope effect is observed when PY is varied at a fixed saturating concentration of AcCoA. The unitary value of $^{D_2O}V/K_{AcCoA}$ at a saturating PY concentration indicates either that AcCoA is sticky under these conditions (dissociates more slowly than chemistry occurs), which is also in agreement with the nonrapid equilibrium kinetic mechanism (Scheme 2), or that with PY the kinetic mechanism becomes ordered, with AcCoA binding before PY (*43*).

Enolization and Condensation. Enolization of AcCoA, the first chemical step in the reaction of *Mt*IPMS, is catalyzed by a general base with a pK_a value of 6.7 (Figure 3). The assignment of the active-site base is not an easy task in the case of *Mt*IPMS because of the presence of several strictly conserved ionizable residues in the active site (e.g., Arg80, Glu218, Glu317, Arg318, His379′, and Tyr410′) and the lack of a structure with AcCoA bound. Therefore, we will not speculate on the identity of the active-site base without further mutagenesis data.

We were unable to detect enolization of AcCoA under a variety of conditions, including in the presence of α-hydroxy acid analogues of the substrate. This indicates a strong degree of coupling between the enolization and condensation reactions. The fact that enolization only takes place when the α-keto acid substrate is present indicates that *Mt*IPMS might use a concerted mechanism for enolization and condensation. Concerted mechanisms are a common strategy used by enzymes to avoid the formation of very unstable species, like the carbanionic enolate of AcCoA, and for rate acceleration of enzymatic enolization reactions (e.g., man-

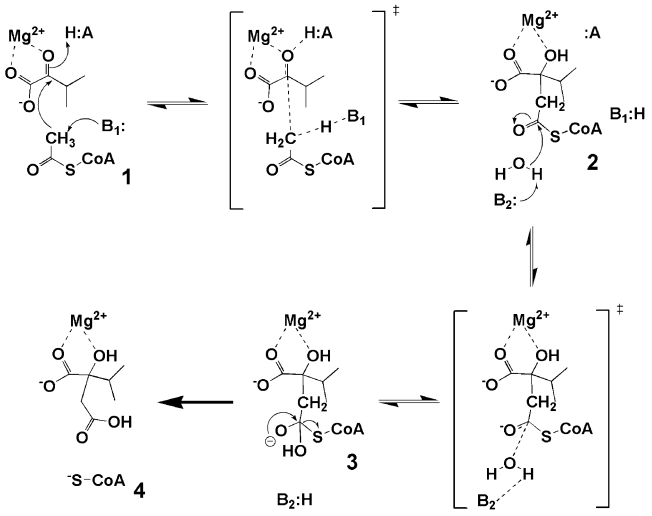

FIGURE 5: Proposed chemical mechanism for *Mt*IPMS-catalyzed reaction. B_1 and B_2 represent the two bases whose ionization are observed in the k_{cat} pH profile. H:A is likely to be Arg80 based on the structure of the E-Zn^{2+}-α-KIV structure (*22*) and may be the additional ionizable group observed in the $k_{cat}/K_{m\ \alpha-KIV}$ pH profile. The acidic ionizable groups observed in the $k_{cat}/K_{m\ AcCoA}$ pH profile cannot be assigned because no structural data on an AcCoA complex exist.

delate racemase uses concerted general acid/base catalysis to promote rate acceleration of the proton abstraction from mandelate) (*44*−*46*). Figure 5 depicts the mechanism that we propose for *Mt*IPMS with a concerted enolization and condensation step. An alternative stepwise mechanism can be easily accommodated by assuming that enolization only occurs when α-KIV is bound and that the enzyme base does not exchange with the solvent from the enolate complex. Malate synthase follows a stepwise mechanism (*47*), but the absence of primary deuterium isotope effects precludes the use of multiple isotope effects in our case. In the case of pig heart CS, the enolization of AcCoA is easily demonstrated; however, enolization was not observed for the *T. acidophilum* CS (*11*), which could indicate that the latter follows a concerted pathway.

In summary, after deprotonation of AcCoA (**1**), condensation takes place more rapidly than reprotonation and the α-hydroxyl group of the intermediate α-isopropylmalyl-CoA (**2**) is either rapidly protonated or stabilized as the alkoxide by Mg^{2+} coordination before release and protonation (Figure 5).

Hydrolysis of α*-Isopropylmalyl-CoA.* After condensation, a second enzymic base also exhibiting a pK_a value of 6.7 abstracts a proton from a water molecule, which attacks the thioester carbon of the intermediate (**2**), forming a short-lived tetrahedral intermediate (**3**). The linear proton inventory obtained indicates that there is only a single proton in flight during the transition state for hydrolysis (Figure 5). In addition, the normal solvent isotope effect observed indicates that the water molecule that is hydrolyzing the thioester intermediate is not bound to the divalent metal, which would be expected to yield inverse solvent isotope effects (*48*). The intermediate **3** then collapses, releasing the two products, CoA (**4**) and α-IPM. With the physiological substrates, this step is not rate-limiting. We do not believe that there is an α-IPM anhydride formed in the reaction cycle of *Mt*IPMS. This conclusion is derived from three major observations. First, there is no incorporation of the ^{18}O label in the carboxylate derived from α-KIV during the reaction (Figure 4), which excludes the possibility of release of an anhydride in solution. Second, *Mt*IPMS is able to hydrolyze a variety of acyl-CoA analogues that cannot undergo cyclization in the absence of α-keto acids (Table 2). Third, inspection of the crystal structure of *Mt*IPMS does not show any space in the active-site pocket for a five-membered ring, without major structural rearrangements (*22*).

Finally, our inability to detect isotope effects with the physiological substrates under a variety of conditions suggests that a step other than chemistry is rate-limiting. This could be caused by slow substrate binding or product dissociation, a conformational change that allows for substrate binding or product release, or a combination of both. Although there are other explanations for the lack of observable isotope effects in carbanion formation, such as very asymmetrical or nonlinear transition states and very fast internal return (*49*), the slow dissociation of the substrates/products seems to fit with our kinetic and mechanistic data.

CONCLUSIONS

*Mt*IPMS is a stable dimer in solution, and this is not affected by the addition of K^+, Mg^{2+}, or the feedback inhibitor L-leucine. The α-keto acid specificity of *Mt*IPMS is narrow, and the acyl-CoA specificity is essentially absolute for AcCoA. *Mt*IPMS is the first Claisen-condensing enzyme characterized to date that does not follow an ordered kinetic mechanism. It follows a nonrapid equilibrium random bi-bi kinetic mechanism, with a preferred pathway to the ternary complex. *Mt*IPMS uses general base chemistry for both deprotonation−condensation and hydrolytic reactions. With the physiological substrates, a step other than chemistry is rate-limiting for the overall reaction. Using PY, hydrolysis of α-methylmalyl-CoA is partially rate-limiting. Our solvent KIE data argue that the metal is not involved in the activation of the water molecule for hydrolysis. Finally, the α-isopropylmalyl-CoA thioester intermediate is directly hydrolyzed by water.

ACKNOWLEDGMENT

We thank Drs. Jordan Kriakov and William R. Jacobs Jr. for the generous donation of *M. tuberculosis* $H37R_v$ genomic DNA. We also thank Dr. Sean Cahill for his contributions to the NMR experiments, Dr. Michael Brenowitz for assistance with the sedimentation velocity experiments and the interpretation of its results, and Dr. James Errey for his assistance with preparation and purification of dethio-CoA. Finally, the authors thank Mr. Rafael Guimarães da Silva for careful reading of this manuscript and Dr. Argyrides Argyrou for thoughtful discussions.

SUPPORTING INFORMATION AVAILABLE

Initial velocity patterns for *Mt*IPMS and plots showing apparent substrate inhibition by AcCoA (in the presence of saturating concentrations of PY) and α-KV (in the presence of saturating concentrations of AcCoA). This material is available free of charge via the Internet at http://pubs.acs.org.

REFERENCES

1. McAdam, R. A., Weisbrod, T. R., Martin, J., Scuderi, J. D., Brown, A. M., Cirillo, J. D., Bloom, B. R., and Jacobs, W. R., Jr. (1995) In vivo growth characteristics of leucine and methionine auxotrophic mutants of *Mycobacterium bovis* BCG generated by transposon mutagenesis, *Infect. Immun. 63*, 1004−1012.
2. Bange, F. C., Brown, A. M., and Jacobs, W. R., Jr. (1996) Leucine auxotrophy restricts growth of *Mycobacterium bovis* BCG in macrophages, *Infect. Immun. 64*, 1794−1799.
3. Hondalus, M. K., Bardarov, S., Russell, R., Chan, J., and Jacobs, W. R., Jr., and Bloom, B. R. (2000) Attenuation of and protection induced by a leucine auxotroph of *Mycobacterium tuberculosis*, *Infect. Immun. 68*, 2888−2898.
4. de Carvalho, L. P., Argyrou, A., and Blanchard, J. S. (2005) Slow-onset feedback inhibition: Inhibition of *Mycobacterium tuberculosis* α-isopropylmalate synthase by L-leucine, *J. Am. Chem. Soc. 127*, 10004−10005.
5. Umbarger, H. E. (1996) In *Escherichia coli and Salmonella. Cellular and Molecular Biology* (Neidhardt, F. C., Ed.) pp 442−449, ASM Press, Washington, DC.
6. Cole, S. T., Brosch, R., Parkhill, J., Garnier, T., Churcher, C., Harris, D., Gordon, S. V., Eiglmeier, K., Gas, S., Barry, C. E., III, Tekaia, F., Badcock, K., Basham, D., Brown, D., Chillingworth, T., Connor, R., Davies, R., Devlin, K., Feltwell, T., Gentles, S., Hamlin, N., Holroyd, S., Hornsby, T., Jagels, K., Barrell, B. G., et al. (1998) Deciphering the biology of *Mycobacterium tuberculosis* from the complete genome sequence, *Nature 393*, 537−544.
7. Wheeler, P. R., and Blanchard, J. S. (2005) in *Tuberculosis and the Tubercle Bacillus* (Cole, S. T., Eisenach, K. D., McMurray, D. N., and Jacobs, W. R., Jr., Eds.) pp 312−314, ASM Press, Washington, DC.
8. Andi, B., West, A. H., and Cook, P. F. (2004) Kinetic mechanism of histidine-tagged homocitrate synthase from *Saccharomyces cerevisiae*, *Biochemistry 43*, 11790−11795.
9. Smith, C. V., Huang, C. C., Miczak, A., Russell, D. G., Sacchettini, J. C., and Honer zu Bentrup, K. (2003) Biochemical and structural studies of malate synthase from *Mycobacterium tuberculosis*, *J. Biol. Chem. 278*, 1735−1743.
10. Anstrom, D. M., Kallio, K., and Remington, S. J. (2003) Structure of the *Escherichia coli* malate synthase G:pyruvate:acetyl-coenzyme A abortive ternary complex at 1.95 Å resolution, *Protein Sci. 12*, 1822−1832.
11. Kurz, L. C., Drysdale, G., Riley, M., Tomar, M. A., Chen, J., Russell, R. J., and Danson, M. J. (2000) Kinetics and mechanism of the citrate synthase from the thermophilic archaeon *Thermoplasma acidophilum*, *Biochemistry 39*, 2283−2296.
12. Teng-Leary, E., and Kohlhaw, G. B. (1973) Mechanism of feedback inhibition by leucine. Binding of leucine to wild-type and feedback-resistant α-isopropylmalate synthases and its structural consequences, *Biochemistry 12*, 2980−2986.
13. Teng-Leary, E., and Kohlhaw, G. B. (1975) Binding of α-ketoisovalerate to α-isopropylmalate synthase. Half-of-the-sites and all-of-the-sites availability, *Biochim. Biophys. Acta 410*, 210−219.
14. Kohlhaw, G., Leary, T. R., and Umbarger, H. E. (1969) α-Isopropylmalate synthase from *Salmonella typhimurium*. Purification and properties, *J. Biol. Chem. 244*, 2218−2225.
15. Leary, T. R., and Kohlhaw, G. (1970) Dissociation of α-isopropylmalate synthase from *Salmonella typhimurium* by its feedback inhibitor leucine, *Biochem. Biophys. Res. Commun. 39*, 494−501.
16. Wiegel, J., and Schlegel, H. G. (1977) α-Isopropylmalate synthase from *Alcaligenes eutrophus* H 16. II. Substrate specificity and kinetics, *Arch. Microbiol. 112*, 247−254.
17. Wiegel, J., and Schlegel, H. G. (1977) α-Isopropylmalate synthase from *Alcaligenes eutrophus* H 16 I. Purification and general properties, *Arch. Microbiol. 112*, 239−246.
18. Wiegel, J., and Schlegel, H. G. (1977) α-Isopropylmalate synthase from *Alcaligenes eutrophus* H 16. III. Endproduct inhibition and its relief by valine and isoleucine, *Arch. Microbiol. 114*, 203−210.
19. Webster, R. E., and Gross, S. R. (1965) The α-isopropylmalate synthetase of *Neurospora*. I. The kinetics and end product control of α-isopropylmalate synthetase function, *Biochemistry 4*, 2309−2318.
20. Kohlhaw, G. B. (1988) α-Isopropylmalate synthase from yeast, *Methods Enzymol. 166*, 414−423.
21. Chanchaem, W., and Palittapongarnpim, P. (2002) A variable number of tandem repeats result in polymorphic α-isopropylmalate synthase in *Mycobacterium tuberculosis*, *Tuberculosis 82*, 1−6.
22. Koon, N., Squire, C. J., and Baker, E. N. (2004) Crystal structure of LeuA from *Mycobacterium tuberculosis*, a key enzyme in leucine biosynthesis, *Proc. Natl. Acad. Sci. U.S.A. 101*, 8295−8300.
23. Philo, J. S. (1997) An improved function for fitting sedimentation velocity data for low-molecular-weight solutes, *Biophys. J. 72*, 435−444.
24. Jocelyn, P. C. (1987) in *Sulfur and Sulfur Amino Acids* (Jakoby, W. B., and Griffith, O. W., Eds.) pp 44−50, Academic Press, Inc., Orlando, FL.
25. de Carvalho, L. P., and Blanchard, J. S. (2006) Kinetic analysis of the effects of monovalent cations and divalent metals on the activity of *Mycobacterium tuberculosis* α-isopropylmalate synthase, *Arch. Biochem. Biophys.* In press.
26. Dawson, R. M. C., Elliot, D. C., Elliot, W. H., and Jones, K. M. (1991) Oxford University Press, New York.
27. Cleland, W. W. (1982) The use of pH studies to determine chemical mechanisms of enzyme-catalyzed reactions, *Methods Enzymol. 87*, 390−405.
28. Stoll, V. S., and Blanchard, J. S. (1990) Buffers: Principles and practice, *Methods Enzymol. 182*, 24−38.
29. Risley, J., and van Etten, R. (1979) An ^{18}O isotope shift upon ^{13}C NMR spectra and its application to the study of oxygen exchange kinetics, *J. Am. Chem. Soc. 101*, 252−253.
30. Risley, J., and van Etten, R. (1980) ^{18}O isotope effect in ^{13}C nuclear magnetic resonance spectroscopy. 2. The effect of structure, *J. Am. Chem. Soc. 102*, 4609−4614.
31. Skoog, D. A., and West, D. M. (1982) *Fundamentals of Analytical Chemistry*, Saunders College Publishing, Philadelphia, PA.
32. Garcia de la Torre, J., Huertas, M. L., and Carrasco, B. (2000) Calculation of hydrodynamic properties of globular proteins from their atomic-level structure, *Biophys. J. 78*, 719−730.
33. Cleland, W. W. (1977) Determining the chemical mechanisms of enzyme-catalyzed reactions by kinetic studies, *Adv. Enzymol. Relat. Areas Mol. Biol. 45*, 273−387.
34. Segel, I. H. (1993) *Enzyme Kinetics, Behavior and Analysis of Rapid Equilibrium and Steady-State Enzyme Systems*, John Wiley and Sons, Inc., New York.
35. Ferdinand, W. (1966) The interpretation of non-hyperbolic rate curves for two-substrate enzymes. A possible mechanism for phosphofructokinase, *Biochem. J. 98*, 278−283.
36. Risley, J. M., and Etten, R. L. V. (1980) Oxygen-18 isotope effect in carbon-13 nuclear magnetic resonance spectroscopy. 2. The effect of structure, *J. Am. Chem. Soc. 102*, 4609−4614.
37. Risley, J. M., and Etten, R. L. V. (1979) An oxygen-18 isotope shift upon carbon-13 NMR spectra and its application to the study of oxygen exchange kinetics, *J. Am. Chem. Soc. 101*, 252−253.
38. Tong, E. K., and Duckworth, H. W. (1975) The quaternary structure of citrate synthase from *Escherichia coli* K12, *Biochemistry 14*, 235−241.
39. Bar-Tana, J., and Cleland, W. W. (1974) Rabbit muscle phosphofructokinase. II. Product and dead end inhibition, *J. Biol. Chem. 249*, 1271−1276.
40. Williams, J. W., and Northrop, D. B. (1978) Kinetic mechanisms of gentamicin acetyltransferase I. Antibiotic-dependent shift from rapid to nonrapid equilibrium random mechanisms, *J. Biol. Chem. 253*, 5902−5907.
41. Williams, K. R., and Schofield, P. (1977) Kinetic mechanism of tRNA nucleotidyltransferase from *Escherichia coli*, *J. Biol. Chem. 252*, 5589−5597.
42. Fersht, A. (1999) *Structure and Mechanism in Protein Science*, W.H. Freeman and Company, New York.
43. Cook, P. F. (1991) in *Enzyme Mechanism from Isotope Effects* (Cook, P. F., Ed.) pp 203−207, CRC Press, Inc., Boca Raton, FL.
44. Gerlt, J. A., Kozarich, J. W., Kenyon, G. L., and Gassman, P. G. (1991) Electrophilic catalysis can explain the unexpected acidity of carbon acids in enzyme-catalyzed reactions, *J. Am. Chem. Soc. 113*, 9667−9669.
45. Gerlt, J. A., and Gassman, P. G. (1993) Understanding the rates of certain enzyme-catalyzed reactions: Proton abstraction from carbon acids, acyl-transfer reactions, and displacement reactions of phosphodiesters, *Biochemistry 32*, 11943−11952.

46. Mitra, B., Kallarakal, A. T., Kozarich, J. W., Gerlt, J. A., Clifton, J. G., Petsko, G. A., and Kenyon, G. L. (1995) Mechanism of the reaction catalyzed by mandelate racemase: Importance of electrophilic catalysis by glutamic acid 317, *Biochemistry 34*, 2777−2787.
47. Clark, J. D., O'Keefe, S. J., and Knowles, J. R. (1988) Malate synthase: Proof of a stepwise Claisen condensation using the double-isotope fractionation test, *Biochemistry 27*, 5961−5971.
48. Quinn, D. M., and Sutton, L. D. (1991) In *Enzyme Mechanism from Isotope Effects* (Cook, P. F., Ed.) pp 73−126, CRC Press, Inc., Boca Raton, FL.
49. Buncel, E., and Dust, J. M. (2003) *Carbanion Chemistry. Structure and Mechanisms*, Oxford University Press, New York.

BI0606602